Li Mobility in the Orthorhombic $Li_{0.18}La_{0.61}TiO_3$ Perovskite Studied by NMR and Impedance Spectroscopies

M. A. París and J. Sanz*

Instituto de Ciencia de Materiales de Madrid (CSIC), Cantoblanco, 28049 Madrid, Spain

C. León and J. Santamaría

Departamento de Física Aplicada III, Facultad de Ciencias Físicas, Universidad Complutense de Madrid, 28040 Madrid, Spain

J. Ibarra and A. Várez

Departamento de Materiales, Escuela Politécnica Superior, Universidad Carlos III de Madrid, 28911 Leganés, Spain

Received August 6, 1999. Revised Manuscript Received March 23, 2000

Electrical conductivity and NMR relaxation times (T_1 and T_2) have been determined in the $Li_{0.18}La_{0.61}TiO_3$ perovskite. At room temperature, the unit cell constants are $a = 3.865(1)$, $b = 3.876(1)$, and $c = 7.788(2)$ Å and the space group $Pmmm$ (orthorhombic). In this doubled perovskite, the Rietveld analysis of the X-ray powder pattern showed that La ions occupy preferentially one type of sites ($z/c = 0$), and Li and vacancies accommodate with the remaining La at the second site ($z/c = 0.5$). From this fact, Li motion should be favored in the plane *ab*; however, exchanges of Li between contiguous layers are detected above 200 K by NMR spectroscopy. From T_1 and T_2 NMR data, two main relaxation mechanisms have been detected, which have been ascribed to localized exchanges (200−273 K) and extended motions of Li (above 273 K). The dc conductivity shows a non-Arrhenius temperature dependence, and local activation energies of 0.41 and 0.26 eV were obtained in the low- and high-temperature ranges, respectively. Both NMR and electrical conductivity relaxations are described by "stretched exponential" functions, characteristic of correlated ion motions.

1. Introduction

Interest in solid electrolytes for use in solid-state batteries has increased in recent years. Lithium-based systems are attractive due to high energy densities and high open circuit potentials. In particular, lithium lanthanum titanates with perovskite structure exhibit one of the highest conductivities reported at room temperature (10^{-3} S/cm).[1] In this family of compounds, the poor coordination of Li and the presence of abundant vacant equivalent sites enhances Li mobility.[1,2] On the other hand, ionic conductivity depends on cations occupying A sites of the perovskite; lanthanide ions with a smaller radius than La depress Li mobility, while Sr with a larger radius, improves slightly the conductivity.[2,3] The progressive substitution of Li for La in $Li_{3x}La_{2/3-x}TiO_3$ perovskites reduces slightly the unit cell size but increases the conductivity.[4] At present, the influence of the structure on ionic conductivity has not been established, being necessary additional work to understand the causes that enhance the Li mobility in these compounds.

NMR spin−lattice relaxation (SLR) and electrical conductivity relaxation (ECR) techniques have been often proposed to study cation mobility in solids. In lithium lanthanum perovskites, relaxation functions describing either SLR or ECR show significant deviations from the simple exponential behavior, characteristic of ideal Bloembergen−Purcell−Pound (BPP) or Debye-like relaxations.[5,6] These deviations have been described using stretched exponentials of the Kohlrausch−Williams−Watts (KWW) form,[7] $f(t) = \exp[-(t/\tau)^{\beta}]$, with $\beta \approx 0.4$ taking into account of correlation effects in ion motion. Activation energies corresponding to short- and long-range motions of Li in these perovskites verified the expression $E_m = E_M\beta$,[5] deduced from the coupling and jump relaxation models.[8,9] Alternatively, SLR and ECR data taken in different perovskites

(1) Inaguma, Y.; Chen, L.; Itoh, M.; Nakamura, T.; Uchida, T.; Ikuta, M.; Wakihara, M. *Solid State Commun.* **1993**, *86*, 689.
(2) Inaguma, Y.; Chen, L.; Itoh, M.; Nakamura, T. *Solid State Ionics* **1994**, *70/71*, 196.
(3) Itoh, M.; Inaguma, Y.; Jung, W.; Chen, L.; Nakamura, T. *Solid State Ionics* **1994**, *70/71*, 203.
(4) Kawai, H.; Kuwano, J. *J. Electrochem.* **1994**, *141*, L78.
(5) León, C.; Lucía, M. L.; Santamaría, J.; París, M. A.; Sanz, J.; Várez, A. *Phys. Rev. B* **1996**, *54*, 184.
(6) Emery, J.; Buzare, J. Y.; Bohnke, O.; Fourquet, J. L. *Solid State Ionics* **1997**, *99*, 41.
(7) Kohlrausch, R. *Ann. Phys. Lpz.* **1847**, ***72***, 393.
(8) Ngai, K. L. *Comments Solid State Phys.* **1979**, *9*, 121; **1980**, *9*, 141. Ngai, K. L. *Effects of Disorder on Relaxational Processes*; Springer-Verlag: Berlin, 1994.
(9) Funke, K. *Prog. Solid State Chem.* **1993**, *22*, 111.

10.1021/cm9911159 CCC: $19.00
Published on Web 05/16/2000

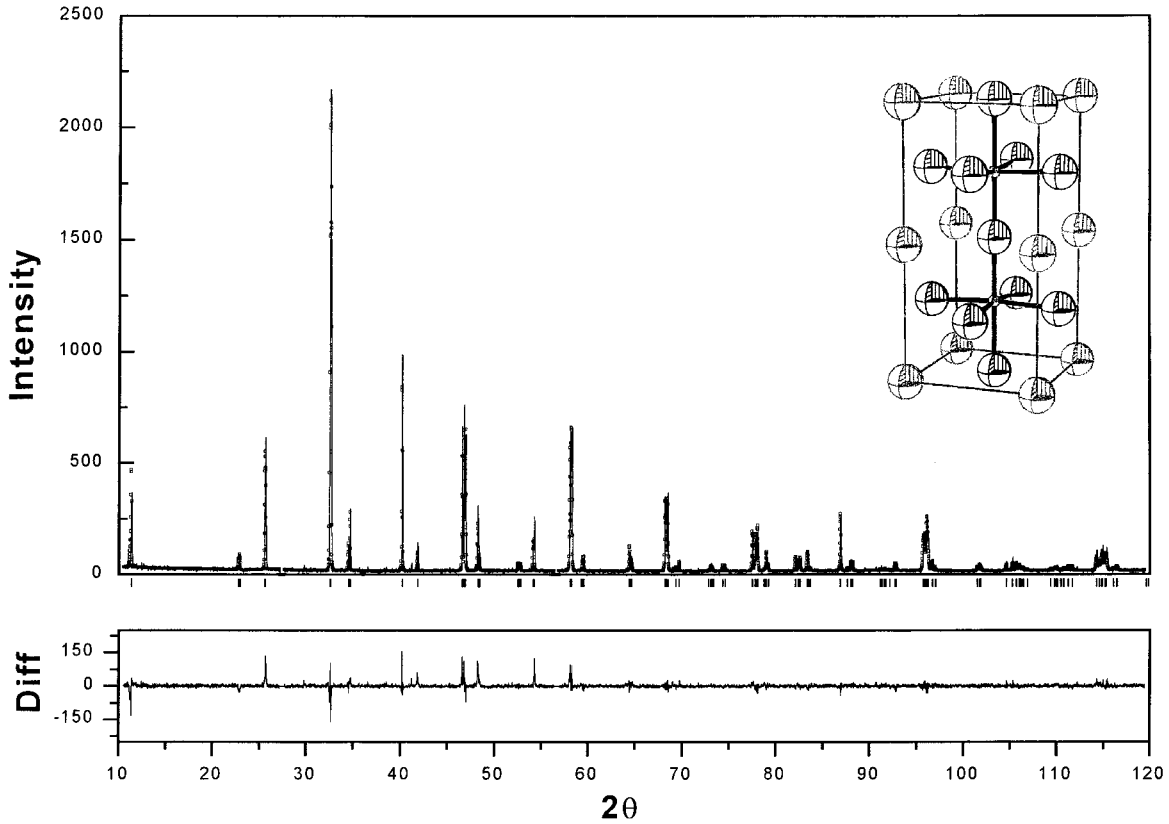

Figure 1. Observed, calculated, and difference X-ray diffraction plots of $Li_{0.18}La_{0.61}TiO_3$. A schematic view of the orthorhombic unit cell, deduced from the Rietveld analysis, is included as an inset.

were interpreted by assuming the existence of a distribution of correlation times for Li motions.[10]

In this paper, we present the study of the orthorhombic $Li_{0.18}La_{0.61}TiO_3$ perovskite by NMR and impedance spectroscopies. In this compound, the Rietveld analysis of the XRD pattern allowed the structural features to be determined and the NMR technique the study of Li−perovskite interaction. Finally, NMR and impedance techniques have been used to study the lithium mobility and from that to determine the most probable lithium motion mechanism.

2. Experimental Section

Samples were prepared by heating a stoichimetric mixture of high purity Li_2CO_3, La_2O_3, and TiO_2 reagents at 1425 K. The reacted powder was pelleted and fired at 1625 K in air for 6 h and then slowly cooled to room temperature. The metal ratio was determined by inductively coupled plasma spectroscopy (ICP) using a JY-70 PLUS spectrometer.

The X-ray powder patterns were collected between 300 and 900 K in a Phillips X-Pert diffractometer with ($\theta/2\theta$) Bragg−Brentano geometry using the Cu Kα radiation ($\lambda = 1.5418$ Å). An Anton Paar camera was used for the experiments at variable temperatures. The data were taken with a 0.5° divergence slit, a receiving slit of 0.01°, and a set of Soller slits with axial divergence of 1°. For phase purity assessment and indexing purposes, data were recorded between $2\theta = 13$ and 70°. For Rietveld structural refinement, data were collected at room temperature between $2\theta = 13$ and 120°, with 0.02° step size and 10 s counting time.

The ^{7}Li NMR spectra were obtained between 200 and 350 K in a MSL-400 Bruker spectrometer working at 155.45 MHz. Spectra were taken after irradiation of the sample with a $\pi/2$ pulse (3 μs). The number of scans was 30 and the time between accumulations was 10 s. Determination of T_1 values was done between 100 and 500 K by using the classical ($\pi-\tau-\pi/2$) sequence in a SXP 4/100 Bruker spectrometer, working at 10.6 MHz. Analysis of spectra was carried out with the Winfit program (Bruker). This program allows the position, line width, and intensity of the components to be determined by using a nonlinear iterative least-squares method. However, quadrupole constants C_Q and η must be determined by a trial and error procedure.

Admittance spectroscopy was applied in the frequency range 20 Hz to 30 MHz using automatically controlled HP 4284A and HP 4285A precision LCR meters, at temperatures comprised between 150 and 500 K. The samples were cylindrical pellets 5 mm in diameter and 0.7 mm thick on whose faces gold electrodes were deposited by evaporation. Measurements were conducted under a N_2 flow to ensure an inert atmosphere.

3. Results

3.1. X-ray Data. The X-ray diffraction pattern of the $Li_{0.18}La_{0.61}TiO_3$ sample, recorded with the Cu Kα radiation is presented in Figure 1. Peaks indexing was done by using the Treor program according to an orthorhombic cell of parameters $a = 3.865(1)$, $b = 3.876(1)$, and $c = 7.788(2)$ Å. Splittings associated with differentiation of a and b axis (020, 200; near 46.5°), (122, 212; near 58°), (024, 204 near 68°), etc. excluded the indexation of the XRD pattern with the tetragonal unit cell ($P4/mmm$ symmetry) proposed elsewhere.[11,12]

From the ideal structure of perovskite, atom positions compatible with the $Pmmm$ symmetry were deduced.

(10) Bohnke, O.; Emery, J.; Veron, A.; Fourquet, J. L.; Buzare, J. Y.; Florian, P.; Massiot, D. *Solid State Ionics* **1998**, *109*, 25.

(11) Robertson, A. D.; Garcia Martín, S.; Coats, A.; West, A. R. *J. Mater. Chem.* **1995**, *5*, 1405.

(12) Fourquet, J. L.; Duroy, H.; Crosnier-Lopez, M. P. *J. Solid State Chem.* **1996**, *127*, 283.

Table 1. Crystal Data for $Li_{0.18}La_{0.61}TiO_3$ Deduced from the XRD Pattern Taken at 295 K (Space Group *Pmmm*; *Z* = 2; *a* = 3.865(1), *b* = 3.876(1), and *c* = 7.788(2) Å)[a]

atom	*x*/*a*	*y*/*b*	*z*/*c*	sites	frac.	$U_{iso} \times 100$
La1	0	0	0	1 a	0.92(1)	0.14(4)
La2	0	0	0.5	1 c	0.28(1)	0.70(10)
Ti	0.5	0.5	0.2654(5)	2 t	1.0	0.72(7)
O1	0.5	0.5	0	1 f	1.0	1.70(19)
O2	0.5	0.5	0.5	1 h	1.0	1.61(19)
O3	0.5	0	0.2238(10)	2 s	1.0	1.90(15)
O4	0	0.5	0.2795(10)	2 r	1.0	1.95(15)

[a] $R_F = 6.4\%$, $R_F^2 = 10.2\%$, $R_p = 10.2\%$ and $R_{wp} = 13.5\%$ and $\chi^2 = 2.9$.

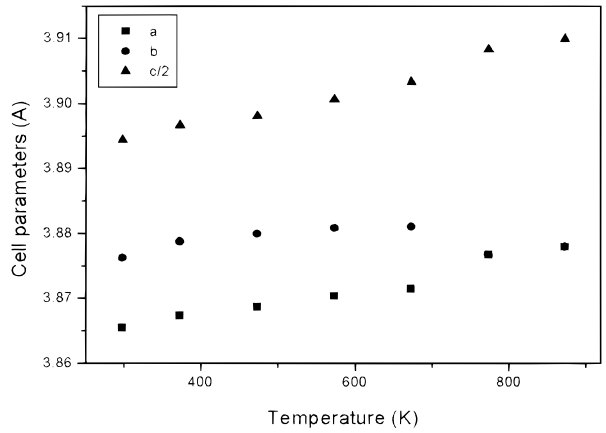

Figure 2. Plot of cell parameters (*a*, *b*, and *c*) vs temperature for $Li_{0.18}La_{0.61}TiO_3$.

With this model, the structure was refined by using the GSAS program (Rietveld method). The common overall parameters, histogram scale factor, background coefficients, unit cell parameters, zero shift, and pseudo Voigt coefficients corrected for asymmetry were deduced. In a second stage, positional parameters and sites occupation were analyzed. Taken into account the weak Li scattering factor, only La occupation of two structural sites was refined. Obtained results conform with the nominal composition of the sample. Introduction of anisotropic thermal factors for oxygen atoms did not improve significantly the fitting. Final agreement factors obtained were $R_F = 6.4\%$, $R_F^2 = 10.2\%$, $R_P = 10.2\%$, $R_{wp} = 13.5\%$, and $\chi^2 = 2.9$. The resulting fitting of the X-ray pattern is given in the Figure 1. Refined unit cell and atomic parameters are given in Table 1.

From the analysis of unit cell parameters with temperature, it is observed that the thermal expansion is anisotropic and that of the *c* axis is higher than those of the *a* and *b* axes (Figure 2). At temperatures $T > 673$ K, differences between *a* and *b* parameters become lower; finally, at 773 K the X-ray pattern was indexed as tetragonal ($a = b = 3.876$ and $c = 7.816$ Å). The same observation was reported by Uchino et al.[13] in $La_{0.66}TiO_3$; however, the temperature at which this transformation is detected, was lower (573 K).

3.2. RMN Data. ^{7}Li NMR spectra ($I = 3/2$) consist of a central line ($1/2$, $-1/2$ transition) and a broad pattern ($-3/2$, $-1/2$ and $1/2$, $3/2$ transitions) associated with the quadrupolar interaction of nuclei with electric field gradients (EFG) at cation sites. ^{7}Li NMR spectra of $Li_{0.18}La_{0.61}TiO_3$, recorded between 180 and 360 K, are given in Figure 3. At 180 K, the ^{7}Li NMR spectrum is formed by a single line at the resonance frequency. When the sample is heated above 200 K, the central line narrows and satellite transitions are resolved, their intensity increasing with temperature. In the temperature range analyzed, the outer transitions pattern was reproduced considering that Li ions occupy sites with axial symmetry ($\eta = 0$). Finally, the quadrupolar constant C_Q shows a nonlinear decrease from 100 to 30 kHz when the sample is heated between 220 and 500 K (Figure 4).

Below 200 K, the central line is mostly Gaussian and the line width does not change appreciably, indicating that the Li mobility is low. The second moment of the NMR spectrum recorded at 180 K, 10^7 s^{-2}, was calculated from the spin−spin relaxation time using the expression: $\langle \Delta\omega^2 \rangle = 2/(T_2)^2$. Since the line width of the spectrum is mainly due to dipole interactions, the second moment was used to estimate the average distance Li−Li. On the basis of a random distribution of lithium, a value of 3.7 Å was deduced from the Van Vleck's expression,[14] which is near to the distance between A sites of the perovskite ($a_p = 3.8$ Å).

A cancellation of dipole Li−Li interactions happens when the correlation time of the Li motion, τ, is smaller than $\langle \Delta\omega^2 \rangle^{-1/2}$ (motional narrowing effect). This fact produces the decrease observed between 180 and 220 K in the T_2^{-1} curve (Figure 5). In the same plot, it can also be observed that T_2^{-1} remains unchanged between 220 and 273 K and decreases above 273 K. Above 200 K, the fitting of the spectra requires the presence of two central components with different line widths (Table 2). The observed evolution of T_2^{-1} with temperature suggests the existence of two stages for the Li motion: the first stage starting at 200 K and the second one at 273 K. In the second stage, the Li motion seems to be more extended and the cancellation of the dipolar Li−Li interactions is more efficient. At the same time, quadrupole constants continue to decrease with temperature. Above 400 K, external field inhomogeneities are responsible for the nondecrease of T_2^{-1} at high temperatures.

The temperature dependence of spin−lattice relaxation rate, T_1^{-1}, measured at 10 MHz, is also given in Figure 5. Variation of T_1^{-1} vs $1000/T$ displays a maximum at 273 K with different slopes in the two sides of the maximum. Spin−lattice relaxation rate, T_1^{-1}, is related to the SLR relaxation function through the expression

$$T_1^{-1}(\omega_L, T) = C[J(\omega_L, T) + 4J(2\omega_L, T)] \qquad (1)$$

where $J(\omega_L, T)$ is the spectral density function, *C* is a constant depending of the nuclear interaction, responsible for the relaxation process, and ω_L is the Larmor frequency. From the maximum value of T_1^{-1} a value of $C = 2 \times 10^{10}$ s^{-2} was deduced. In solids, three major mechanisms cause the spin−lattice relaxation of nuclei:[14,15] (1) dipole interactions between nuclei, (2) quadrupole interactions between nuclei and electric field gradients (EFG), and (3) interactions with paramagnetic

(13) Abe, M.; Uchino, K. *Mater. Res. Bull.* **1974**, *9*, 147.

(14) Abragam, A. *The Principles of Nuclear Magnetism*; Oxford University Press: Oxford, 1961.

(15) Fukushima, E.; Roeder, S. B. W. *Experimental Pulse NMR: A Nuts and Bolts Approach*; Addison-Wesley: New York, 1981.

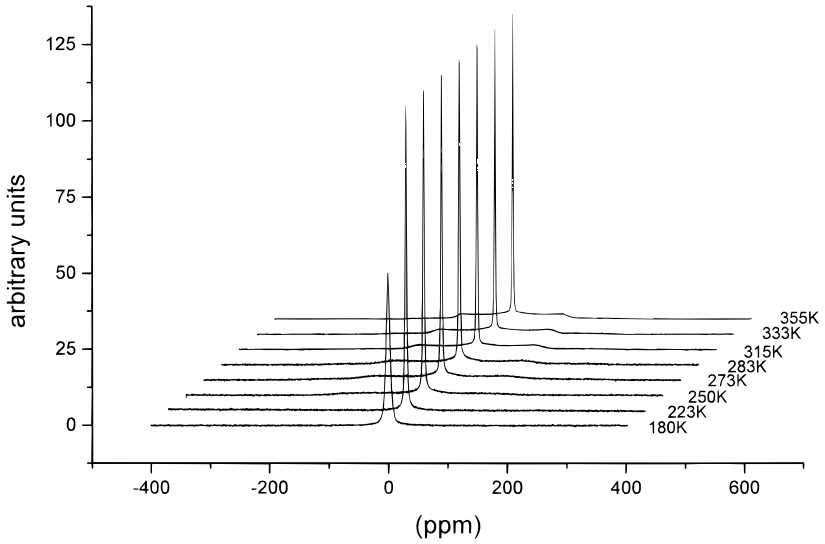

Figure 3. ^{7}Li NMR spectra of $Li_{0.18}La_{0.61}TiO_3$ recorded at increasing temperatures with the single pulse technique.

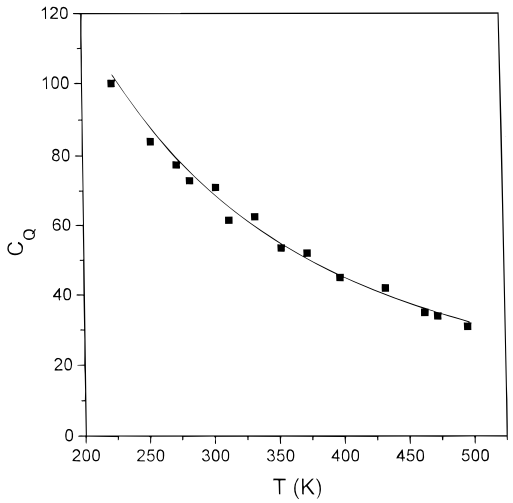

Figure 4. Temperature dependence of the quadrupole C_Q constants. Values were determined from fitting of ^{7}Li NMR spectra.

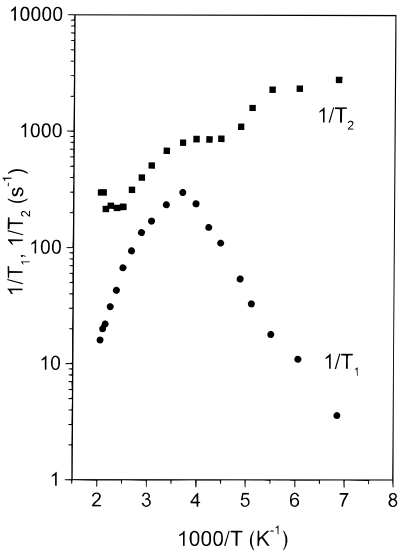

Figure 5. Evolution of NMR relaxation rates T_1^{-1} and T_2^{-1} with the inverse of temperature. T_1 values were determined with the $\pi-\tau-\pi/2$ technique.

centers. If the SLR rate was dominated by dipole interactions between Li, the C value obtained from the fitting of the T_1^{-1} data would be $C = 5 \times 10^7$ s^{-2}, which is 2 orders of magnitude lower than the experimental one. On the other hand, if quadrupole interactions are responsible for the nuclear relaxation, the C constant can be expressed as $C = (2\pi^2/5)C_Q^2$, where C_Q is determined from spectra recorded at low temperatures. From the experimental C value, a $C_Q = 80$ kHz was obtained that is near to 100 kHz, deduced from spectra. Finally, the existence of paramagnetic impurities would produce a significant broadening of the spectrum, that was not observed experimentally. From the above considerations, it can be concluded that the relaxation of Li is mainly dominated by fluctuating EFG, produced during the Li motion.

At the temperature of the maximum of T_1^{-1} curve, the correlation time τ of the Li motion satisfies the relation $\omega_L\tau \approx 1$. From this fact, the correlation time will be $\tau \approx 10^{-8}$ s at 275 K, indicating that Li motion is already important. A deeper analysis of the T_1^{-1} curve shows that a second maximum with a lower intensity could be present at 333 K, confirming the existence of two stages in Li motion deduced from T_2^{-1} data. Activation energies deduced from both sides of the maximum are 0.16 eV (low temperatures side) and 0.25 eV (high temperatures side). Below 200 K, T_1^{-1} values decrease with a lower slope, indicating the possible existence of a third mechanism. A discussion of relaxation mechanisms will be done later.

Table 2. NMR Parameters Deduced from ^{7}Li NMR Spectra[a]

T (K)	δ^b (ppm)	$C_Q{}^b$ (kHz)	η^b	I^b (%)	I^c (%)	δ^c (ppm)
180				0	100	2.2
200				0	100	2.2
223	2.5	100	0.1	20	80	2.1
250	2.5	86	0.1	42	58	2.0
260	2.5	82	0.1	58	42	2.1
273	2.5	76	0.1	63	37	2.0
283	2.5	72	0.1	65	35	2.0
315	2.0	64	0.0	66	34	2.1
333	2.0	59	0.0	69	31	2.2

[a] The estimated errors on positions δ are 0.3 ppm, and those on C_Q and η constants, 1 kHz and 0.1, respectively. Relative errors on integrated intensities are 5%.

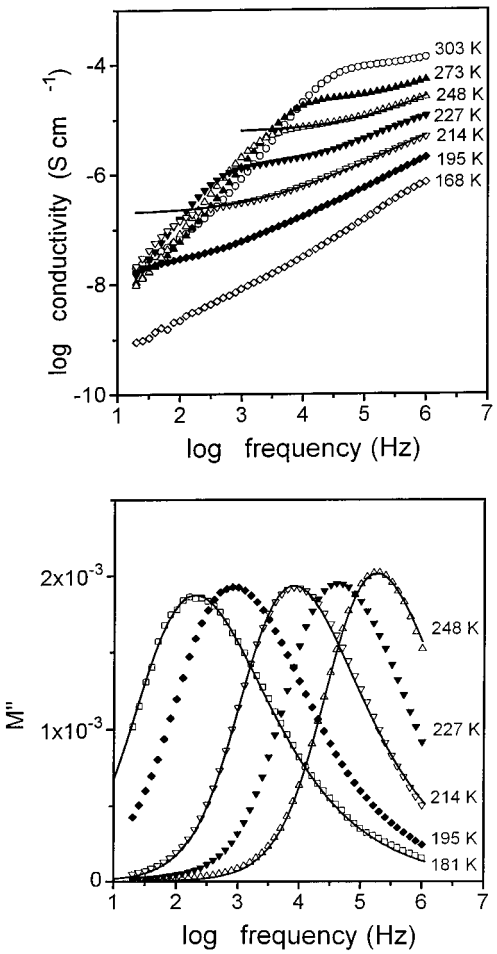

Figure 6. Plot of the real part of the conductivity (a) and the imaginary part of the electric modulus (b) vs frequency. Solid lines of Figure 6a are fits to expression 2 and those of Figure 6b fits to a KWW behavior according to expressions 3 and 4 of the text.

3.3. Electrical Conductivity Relaxation. The frequency dependence of the real part of the conductivity is presented in Figure 6a. The conductivity shows a low-frequency plateau and a crossover to a power law dependence at higher frequencies. This frequency dependence can be described according to a complex conductivity:

$$\sigma^*(\omega) = \sigma_{dc}[1 + (i\omega/\omega_p)^n] \qquad (2)$$

where σ_{dc} is the dc conductivity, ω_p is a crossover frequency, and the exponent $n \approx 0.6$ is related to the degree of correlation in Li ions motion. The decrease of the conductivity observed at lower frequencies and higher temperatures is due to blocking of ions at grain boundaries. The frequency ω_p verifies the relation $\omega_p = \sigma_{dc}/\epsilon_\infty$.[16] It is worth noting that expression 2 is only valid for a temperature−frequency window such that the exponent n is constant. Departures from this behavior are observed when the frequency is increased[17] or the temperature is reduced.[18]

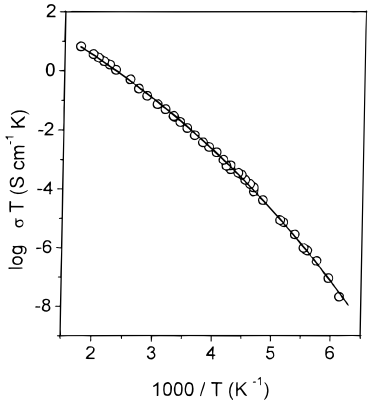

Figure 7. Dc conductivity vs 1000/T showing the non-Arrhenius behavior. Activation energies of 0.41 and 0.26 eV are obtained from Arrhenius local fits of the curve in the 180−250 and 370−523 K temperature ranges.

The dispersive behavior of the conductivity in the frequency domain can be interpreted in terms of a KWW relaxation function $\phi(t)$, which takes the form of a stretched exponential:

$$\phi(t) = \exp[-(t/\tau)^\beta] \qquad (3)$$

where τ is a temperature dependent relaxation time, inversely proportional to the dc conductivity, and $\beta = 1 - n$. From this fact, the electric modulus can be expressed as a function of the time derivative of the ECR relaxation function, through the expression:

$$M^*(\omega) = \frac{1}{\epsilon_\infty}\left[1 - \int_0^\infty \left(-\frac{d\phi}{dt}\right) e^{-i\omega t}\, dt\right] \qquad (4)$$

which allows the relaxation function in the time domain to be determined from experimental data measured in the frequency domain. Figure 6b, shows the imaginary part of the modulus vs the frequency at several temperatures. Nearly temperature-independent β values close to 0.4 have been obtained, confirming that the relationship $\beta = 1 - n$ holds in this system.

On the basis of the scaling properties of the conductivity plots for different temperatures and ion concentrations, conductivity formalism has been recently proposed to be the most adequate to describe the dynamics of ion transport.[19,20] In analyzed perovskites, conductivity plots obtained at different temperatures can be normalized into a single master curve, indicating that a distribution of relaxation times can hardly explain the departure from the Debye behavior.

Dc conductivity data have been obtained from conductivity plots fitting to expression 2. The temperature dependence of the dc conductivity over the whole temperature range is clearly non-Arrhenius (Figure 7), but Arrhenius local fits of the form $\sigma_{dc}T = \sigma_\infty \exp(-E_\sigma/kT)$ yield activation energies, E_σ, of 0.41 eV in the low temperatures (180−250 K) and 0.26 eV in the high temperatures (370−523 K) ranges.

4. Discussion

The X-ray diffraction pattern of $Li_{0.18}La_{0.61}TiO_3$ displays the same features as those reported by Uchino et

(16) León, C.; Lucía, M. L.; Santamaría, J. *Phys. Rev. B* **1997**, *55*, 882.
(17) Cramer, C.; Funke, K.; Saatkamp, T. *Philos. Mag. B* **1995**, *71* (4), 701.
(18) Lee, W. K.; Liu, J. F.; Nowick, A. S. *Phys. Rev. Lett.* **1991**, *67*, 1559.
(19) Roling, B.; Funke, K.; Ingram, M. *Phys. Rev. Lett.* **1998**, *78*, 2160.
(20) Sidebottom, D. L. *Phys. Rev. Lett.* **1999**, *82*, 3653.

al.[13] for $La_{0.66}TiO_3$. From the structural analysis carried out in our sample, it was deduced that the orthorhombic *Pmmm* space group is the best in reproducing the X-ray pattern (Figure 1). This is the first time that the orthorhombic symmetry is observed in $Li_{3x}La_{2/3-x}TiO_3$ perovskites. In our sample, lattice constants are a = 3.865(1), b = 3.876(1), and c = 7.788(2) Å and the volume of unit cell doubles that of the ideal cubic perovskite. From Rietveld analysis, La occupies preferentially one crystallographic site (z/c = 0) and the remaining La, Li and vacancies accommodate at the second site (z/c = 0.5). Structural features deduced in this work are similar to those obtained by Fourquet et al. in tetragonal $Li_{3x}La_{2/3-x}TiO_3$ perovskites, with $0.06 < x < 0.14$.[12] Similar characteristics were also reported by MacEachern in the orthorhombic $La_{0.66}TiO_3$;[21] however, space group (*Pban*) and unit cell (a = 5.461(1), b = 5.482(1), and c = 7.759(3) Å) differ from those obtained here. In both cases, octahedral tiltings in the plane *ab* or along the *c* axis are small, indicating small deviations with respect to the usual *P*4/*mmm* structure reported in other perovskites.[11,12] In this structure, Ti atoms are displaced from the center of octahedral cavities toward the z/c = 0.5 layer, perhaps to compensate for the asymmetric distribution of charges around octahedra (see Table 1 and Figure 1).

One interesting point in $Li_{3x}La_{2/3-x}TiO_3$ perovskites is the poor coordination of Li ions in sites A, resulting from the different cation radii of La and Li ions. The absence of outer ($^1/_2$, $^3/_2$ and $-^1/_2$, $-^3/_2$) transitions in ^{7}Li NMR spectra recorded at low temperatures suggests the existence of irregular sites, with important quadrupole constants, for Li in A cavities of the perovskite that difficults detection of quadrupolar patterns (Figure 3). In fact, the first relaxation detected below 180 K could correspond to the hopping of Li between sites of the perovskite having similar C_Q constants. However, as the mean distance between contiguous Li does not change significantly during this motion, the line width of the central transition (:: T_2^{-1}) does not change appreciably (Figure 5).

The existence of square windows relating contiguous A sites must limit the long-range mobility of Li in perovskites. A calculation of O−O distances in these windows, shows that in all cases they are lower (3.87−3.90 Å) than required for Li to move through. For that, O−O distances across the diagonal should be higher that, 3.96 Å, corresponding to Li in a planar 4-fold coordination (Li−O ≈ 1.99 Å). However, as deduced from NMR spectra, the limiting effect of structural windows decreases considerably when temperature increases above 200 K. When the Li mobility increases, anisotropic interactions are partially averaged and quadrupole outer transitions are resolved. At the same time, mobility reduces the Li−Li dipolar interactions, producing the decrease observed on the line width of the central transition of NMR spectra.

An analysis of the central line shape of NMR patterns, shows the existence of two components that correspond to species with different mobility. More mobile species display a single narrow line ($C_Q \approx 0$) and less mobile species display a broaden quadrupole pattern ($C_Q \approx 100$ kHz). In the orthorhombic perovskite analyzed, the amount of Li and vacancies in the plane z/c = 0.5 is clearly higher than in z/c = 0 (see Table 1). From this fact, mobility of Li should be favored in the plane *ab* with respect to the perpendicular *c* axis (Figure 8).[22] On the basis of these facts, the intense narrow line detected at 220 K has been ascribed to Li moving in the plane z/c = 0.5 (80%) and the second one to Li with restricted mobility in the plane z/c = 0 (20%) (Table 2).

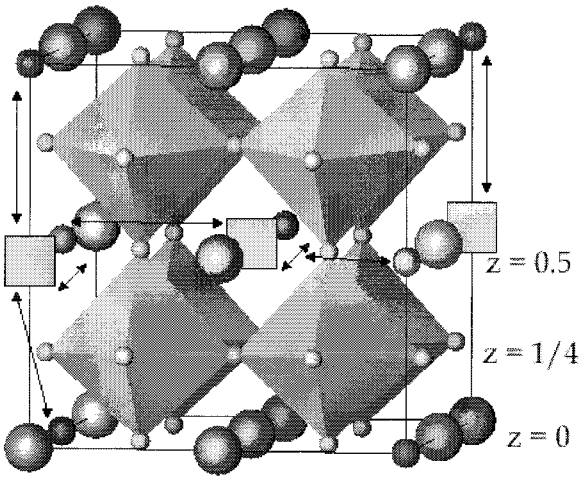

Figure 8. Schematic view of $Li_{0.18}La_{0.61}TiO_3$ structure, illustrating cation distribution in contiguous planes of the perovskite. (Symbols: ○ stands for La, ○ for Li, and □ for vacancies). Possible hops between neighbors sites of the same or adjacent layers are illustrated.

The relaxation mechanism, detected between 220 and 273 K in the T_1^{-1} curve, has been assigned to localized exchanges of Li between contiguous sites of the perovskite. As stated before, Li motion would be favored in the plane *ab*; however, the observed increase on the intensity of outer transitions with temperature, indicates the existence of exchange processes along *c* axis, between Li ions that occupy contiguous planes of the perovskite. On the bases of a fast exchange between these two sites, experimental C_Q values should be given by the expression:

$$C_Q = (n_1 C_Q^{(1)} + n_2 C_Q^{(2)})/(n_1 + n_2) \qquad (5)$$

where $C_Q^{(1)}$ and $C_Q^{(2)}$ are the quadrupole constants and n_1 and n_2 the relative amounts of Li in the two planes. The decrease observed on C_Q (Figure 4), deduced from the broad quadrupole patterns, results from the increase of the amount of mobile species of the plane z/c = 0.5 ($C_Q \approx 0$) that exchange with species of lower mobility of the plane z/c = 0 ($C_Q \approx 100$ kHz). The increase of the outer transitions indicates that at the time scale of the NMR technique (10^{-8} s), a single species with intermediate characteristics is favored. This fact indicates the onset of a tridimensional motion for Li in the perovskite.

Observations supporting the existence of two Li species with different mobility have also been reported by Fourquet et al. in perovskites with Li contents lower than 0.3.[6] However, in samples with Li contents of 0.5, the existence of a unique crystallographic site with low C_Q constant, precluded us the analysis of quadrupolar

(21) MacEachern, M. J.; Dabkowska, H.; Garret, J. D.; Amow, G.; Gong, W.; Liu, G.; Greedan, J. E. *Chem. Mater.* **1994**, *6*, 2092.

(22) Ruiz, A. I.; Lopez, M. L.; Veiga, M. L.; Pico, C. *Solid State Ionics* **1998**, *112*, 291.

patterns and the exchange processes described here.[5,23] In this case, the existence of a unique crystallographic site favored the direct onset of a tridimensional motion of Li.

Activation energies E_m and E_M corresponding to short- and long-range motions of Li can be obtained from the two sides of the T_1^{-1} plot vs the temperature inverse. However, the existence of two nonresolved mechanisms in T_1^{-1} curves hampers the determination of both parameters in each stage of Li motion. From the low-temperatures side of the T_1^{-1} curve a value of $E_m = 0.15$ eV was deduced. This energy can be interpreted in the frame of the coupling model as a microscopic activation energy, free of correlation effects for the Li motion. This microscopic activation energy can be estimated from the conductivity data as the product βE_M,[8,9] being E_M the activation energy of the dc conductivity in the same temperature range. Since in this temperature range $\beta = 0.4$ and $E_M = 0.4$ eV, a value of E_m of 0.16 eV is obtained, in very good agreement with the low-temperature side of the T_1^{-1} plot. A similar activation energy is obtained from the temperature dependence of the dispersive conductivity in this temperature range.[5]

In the 273−500 K range of temperatures, exchange processes between contiguous sites increase, favoring the onset of a more extended motion of Li (Figure 5). At 355 K, 70% of Li ions are involved in three-dimensional exchanges. In this new regime, the activation energy E_M, corresponding to long-range motions of Li, is $E_M = 0.26$ eV which coincides with that determined from conductivity data. Activation energies measured are similar to those obtained in the 250−400 K range by Inaguma et al.[2] in the $Li_{0.16}La_{0.62}TiO_{3.01}$ perovskite.

The good agreement obtained in activation energies deduced from spin lattice and electrical conductivity relaxations leads to the question whether both processes can be described by the same relaxation function. In previous works,[23,24] T_1^{-1} values were reproduced from conductivity data measured in the same frequencies and temperatures. Basically, if the Fourier transform of the ECR relaxation function is given by the expression:

$$\hat{\Phi}(\omega) = \frac{1}{\sigma^*(\omega)/\epsilon_\infty + j\omega} = \frac{1}{(\sigma^*(\omega)/\sigma_{dc})\omega_p + j\omega} \quad (6)$$

with $\sigma^*(\omega)$ standing for the complex conductivity and ϵ_∞ for the high-frequency permittivity; then, the SLR spectral density function would be given by

$$J(\omega) = \frac{1}{(\sigma^*(\omega)/\epsilon_\infty)(T/T_o) + j\omega} = \frac{1}{(\sigma^*(\omega)/\sigma_{dc})\gamma + j\omega} \quad (7)$$

where the mean jump rate of the mobile ions, γ, is connected to the ECR rate through the expression $\sigma_{dc} = \epsilon_\infty(T_o/T)\gamma$. T_o can be approximated by $T_o = nq^2x_o^2/6k_b\epsilon_\infty$, where n is the mobile ions concentration, q their charge, x_o their hopping distance, and k_b the Boltzmann's constant.

Theoretical T_1^{-1} curves, obtained from conductivity measurements at the same frequency (10 MHz), are compared with experimental T_1^{-1} values in Figure 9. Further details about this procedure can be found in ref 24. Calculated T_1^{-1} values fit reasonably well experimental data, indicating that SLR and ECR processes are roughly governed by relaxation functions with similar β exponents and activation energies. However, T_1^{-1} calculated from the conductivity do not reproduce well the maximum at $10^3/T = 4$. We think that the lower resolution obtained in the calculated curve is due to the macroscopic nature of electric measurements in relation to the microscopic information obtained with NMR spectroscopy.

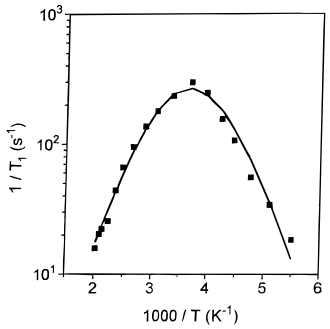

Figure 9. Temperature dependence of T_1^{-1} NMR values taken at 10.6 MHz (■). The continuous line, with 0.26 and 0.16 eV slopes in high- and low-temperature regimes, was calculated from conductivity data taken at the same frequency.

It is important to note that the non-Arrhenius behavior, detected in the orthorhombic $Li_{0.18}La_{0.61}TiO_3$ perovskite, was previously observed in other perovskites with different Li contents and symmetries.[2,5,6] On the other hand, changes observed on conductivity are produced at temperatures considerably lower than those observed in this work (Figure 2) for the orthorhombic−tetragonal transformation (773 K). These observations indicate that the σ_{dc} variation does not depend appreciably on structural distortions produced in perovskites. Moreover, activation energies deduced here are near those reported previously, suggesting that the localized exchanges and extended motions must be operative in all compositions. The small dependence observed on the conductivity with the Li content was interpreted in terms of a variable amount of charge carriers.[2,4]

The observed temperature dependence of the conductivity could be the result of modifications produced on the Li coordination during the sample heating. A progressive opening of square windows, relating contiguous sites of the perovskite, could explain experimental results. To analyze the causes of the conductivity enhancement, a study of the perovskite structure as a function of temperature should be undertaken. It is interesting to remark that a similar behavior to that described here has been reported in other crystalline Li conductors with outstanding electric performance.[25]

4. Conclusions

The Rietveld analysis of the orthorhombic $Li_{0.18}La_{0.61}TiO_3$ showed that La ions occupy preferentially one type of sites ($z/c = 0$) and Li and vacancies accommodate with

(23) León, C.; Santamaría, J.; París, M. A.; Sanz, J.; Ibarra, J.; Varez, A. *J. Non-Cryst. Solids* **1998**, *235−237*, 753.

(24) León, C.; Santamaría, J.; París, M. A.; Sanz, J.; Ibarra, J.; Torres, L. M. *Phys. Rev. B* **1997**, *56*, 5302.

(25) Robertson, A. D.; West, A. R.; Ritchie, A. G. *Solid State Ionics* **1997**, *104*, 1.

the remaining La in the second type of sites ($z/c = 0.5$). The detection of two sites for La in this perovskite is similar to that previously reported in tetragonal perovskites with higher Li contents ($0.06 < x < 0.14$).

The frequency dependence of the electric modulus and conductivity has been described by stretched KWW relaxation functions, with β values near 0.4, characteristic of correlated Li motions. The analysis of the dc conductivity and T_1^{-1} data as a function of temperature displays the complex non-Arrhenius behavior, detected in other lithium lanthane perovskites.

Below 273 K, exchange of Li ions between contiguous structural sites, dominates spectral features of the ^{7}Li NMR spectra. However, above 273 K, a more extended motion of Li is detected in the perovskite. Activation energies for local and extended motions of Li, are respectively 0.41 and 0.26 eV. The identification of structural reasons that limit Li mobility, like structural bottlenecks, requires additional work.

CM9911159